MITSUBISHI ELECTRIC RESEARCH LABORATORIES
http://www.merl.com

Nonlinear Optimal Control Strategies for Buoyancy-Driven Flows in the Built Environment

Nabi, S.; Grover, P.; Caulfield, C.

TR2019-151 December 11, 2019

Abstract

We consider the problem of optimally controlling turbulent buoyancy-driven flows in the built environment, focusing on a model test case of displacement ventilation with a time-varying heat source. The flow is modeled using the unsteady Reynolds-averaged equations (URANS). A direct-adjoint-looping implementation of the nonlinear optimal control problem yields time-varying values of temperature and velocity of the inlet flow that lead to 'optimal' time-averaged temperature relative to appropriate objective functionals in a region of interest. The resulting dynamics of both 'filling' and 'intruding' added layers due to a time-varying source and inlet flow are discussed. The robustness of the optimal solution is demonstrated. It is found that for large enough values of time horizon the optimal steady solution is recovered, while for intermediate values a non-trivial deviation from this optimal steady state design is achieved. The computational framework is flexible, and can be applied to several problems of interest in optimal design and control of indoor airflow.

Journal of Computers and Fluids

Nonlinear Optimal Control Strategies for Buoyancy-Driven Flows in the Built Environment

Saleh Nabi* Piyush Grover † C. P. Caulfield ‡

Abstract

We consider the problem of optimally controlling turbulent buoyancy-driven flows in the built environment, focusing on a model test case of displacement ventilation with a time-varying heat source. The flow is modeled using the unsteady Reynolds-averaged equations (URANS). A direct-adjoint-looping implementation of the nonlinear optimal control problem yields time-varying values of temperature and velocity of the inlet flow that lead to 'optimal' time-averaged temperature relative to appropriate objective functionals in a region of interest. The resulting dynamics of both 'filling' and 'intruding' added layers due to a time-varying source and inlet flow are discussed. The robustness of the optimal solution is demonstrated. It is found that for large enough values of time horizon the optimal steady solution is recovered, while for intermediate values a non-trivial deviation from this optimal steady state design is achieved. The computational framework is flexible, and can be applied to several problems of interest in optimal design and control of indoor airflow.

Keywords— Optimal control; buoyancy-driven flows; transient adjoint method

1 Introduction

Modern buildings are a major contributor to energy consumption in North America, largely due to the Heating, Ventilation and Air Conditioning (HVAC) [1] requirements. It is also evident that indoor airflow greatly affects occupant comfort, health, and productivity. In the past few decades, the field of architectural fluid dynamics has seen considerable advances [2] in the form of better theoretical understanding of buoyancy-driven indoor flows, novel experimental techniques, and advanced numerical methods. There is rising interest in combining these recent advances with modern optimization and control methods [3] for the purpose of optimal design, and control of flow in the built environment. This engineering task has the twin goals of maintaining thermal comfort while reducing energy consumption. The complicated dynamics of airflow within the built environment, and its interaction with occupants, building, and the exterior, necessitate a systematic approach to accomplish this task.

The *adjoint method* [4] has long been identified as the method of choice for optimization in fluid mechanics [5, 6, 7, 8], mostly in the context of shape optimization. In contrast to shape optimization problems, indoor airflow optimization is aimed at obtaining optimal boundary actuation (either steady or time-varying) that leads to desired airflow temperature and velocity distribution characteristics in the domain of interest [9]. In particular, designing and controlling coherent structures in indoor flows to enable 'localized' heating and cooling can result in considerable energy savings by reducing the load [10]. In the past decade, application of systematic optimization and control to indoor airflow has been gaining attention [11, 12, 13, 14, 15]. A parallel but related recent development is the use of nonlinear adjoint optimization techniques to find 'optimal', i.e. minimal energy, perturbations that lead to turbulence in canonical flows [16, 17, 18, 19, 20].

In our previous work [21], we formulated and solved a model test-case problem of *optimal design* to determine *steady* inlet velocity and temperature that optimize a certain cost functional related to achieving a desired temperature distribution in part of a room using the Direct-Adjoint-Looping (DAL) method [17]. That study focused on the fully turbulent mixed-convection regime, resulting from the presence of a line heat source in addition to forced conditioned

*Mitsubishi Electric Research Labs, Cambridge, MA, USA. Corresponding Author. Email: nabi@merl.com

†Mechanical and Materials Engineering, University of Nebraska-Lincoln, NE, USA

‡BP Institute and Department of Applied Mathematics & Theoretical Physics (DAMTP), University of Cambridge, Cambridge, United Kingdom

air from the inlet. Since DNS/LES based numerical optimization is not feasible with reasonable computing resources, we employed Reynolds-Averaged Navier-Stokes (RANS) models to account for interaction between the mean-flow and turbulent eddies. The open source software Open Field Operation and Manipulation (OpenFOAM) [22] was used as the numerical tool to develop our continuous-adjoint based framework. We validated the numerically computed optimal solutions with those obtained by optimizing experimentally-verified analytical reduced-order models for the same problem. Such physics-based reduced-order models for indoor ventilation dynamics have been developed for steady [23] and unsteady [24] natural ventilation, ventilation in the presence of time-varying heat sources [25], exchange flow between adjacent rooms [26, 27], and general unsteady plume dynamics [28], among other phenomena.

Two different approaches for formulating the adjoint of a solver are popular in the literature, the discrete adjoint method and the continuous adjoint method. In the discrete adjoint method, the governing equations are discretised, then transposed with the addition of appropriate source terms in order to arrive at an adjoint code for differentiation [15]. On the other hand in the continuous adjoint method, the adjoint equations are derived analytically from the governing equations and then a numerical solution is constructed by discretization of these adjoint equations. The advantages and disadvantages of these two methods are subject to ongoing research [4] and is not the topic of the paper. Here we choose the continuous adjoint method due to implementational reasons and the associated flexibility of our code being straightforward to adapt to a wide range of cost functions.

In this paper, we extend our previous work by formulating and solving a problem of open-loop time-varying *optimal control* of the velocity and temperature of the inlet air, for the same model of mixed-convection. As a concrete example, we study the problem of optimally maintaining a desired temperature distribution in a part of the room, after a sudden change in strength of the line heat source. The source is assumed to be fixed in the space; however, the results can be extended to cases where the location of the source is altered, provided that the source is away from the inlet or the walls. This example serves as a proof-of-concept of the DAL-based optimal control framework for fully turbulent buoyancy-driven flows with RANS models. The framework we develop has direct application to several related problems of contemporary interest in control of indoor environment. Such problems include intelligent scheduling of air-conditioning equipment using prediction of time-varying occupancy or outdoor conditions, and optimal operation of windows and other openings between various zones, etc.

The performance of a system under open-loop control may degrade greatly under disturbances, hence requiring real-time sensing and feedback control in maintaining the desired (optimal) conditions. Another motivation for the current work is to reduce or eliminate the need for real-time feedback control. The optimal control framework presented here can be adapted to find time-varying open-loop control policies that result in indoor flows that are robust to disturbances, while possibly being slightly sub-optimal with respect to comfort or energy efficiency criteria (when compared with *steady* inlet flow computed in our previous work). Previous results from the field of vibrational control theory [29], and oscillatory flow control [30] lead us to believe that such policies may have periodic or quasi-periodic time dependence.

The rest of the paper is organized as follows. In Section 2, we discuss the numerical model for buoyancy-driven flow with bottom and top vents in the presence of a line heat source of buoyancy. We also compare its transient response with an experimentally-validated analytical model for the case of sudden change in strength of the source. In Section 3, we formulate the optimal control problem, and discuss a implementation of the DAL method to solve this problem. In Section 4, we discuss the results of the optimal control problem, and the dependence of the optimal control policies on various problem parameters. In Section 5, we provide conclusions and sketch out directions for future research.

2 Problem Set-up and Numerical Modeling

Two qualitatively different types of ventilation processes can be straightforwardly defined: the emptying filling box, and forced convection. In the former, the pressure difference between the interior and the exterior of the room drives the flow. In the latter, the inflow is injected to the domain by use of a mechanical device. In either case the outflow is governed by the pressure difference between the interior and the outside.

In either ventilation mode, the thermal plume originating from the heat load interacts with the ambient: the fluid in the vicinity of the heat source rises to the top due to buoyancy forces, and as it ascends, the ambient fluid is entrained into the plume. This leads to a reduction of temperature within the plume. Once the plume reaches to the top it spreads out toward the lateral walls and forms a buoyant layer at the top. The continuous process of entrainment and lateral discharge results in stratification in the upper layer of the domain. Concurrently, the inflow at the bottom induces an upward flow in the bottom layer. There is a significant difference of temperature between the upper layer and the lower layer such that a hypothetical horizontal line divides the two layers in the domain. We

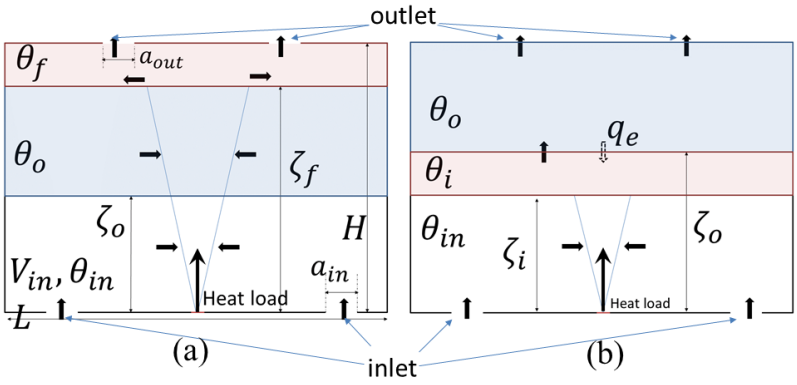

Figure 1: Schematic of the problem of transient flow in case of a) step-up and b) step-down. In panel a) ζ_o is the scaled height of the original layer, ζ_f is the scaled height of the filling layer associated with the 'stepped-up' heat load, H and L are the total height and length of the domain, and a_{in} and a_{out} are the inlet and outlet area respectively. The heat load, modeled as a thermal plume in the current study, is located at the middle of the bottom boundary, and θ_o and θ_f are the original and filling layer scaled temperature of each layer. In panel b) the scaled height of the intruding layer associated with the 'stepped-down' heat load is ζ_i with scaled temperature θ_i, and the possibility of entrainment between the intruding and original layer is quantified by the scaled entrainment flux q_e. θ_{in} and V_{in} are the inlet temperature and velocity, respectively.

refer to the elevation of such a horizontal line as the interface height. The interface height descends until a two-layer steady state is reached.

In this paper we are interested in the response of the flow to a sudden jump in the heat load. Hence, we assume initially there is a steady state in the room for a given heat load and at time $t = 0$. We consider the two cases of sudden increase and decrease in the heat load, which we refer to as step-up and step-down scenarios, respectively. Schematics of both scenarios are shown in Fig. 1. In the step-up scenario, there is a filling layer that descends from the top, and eventually merges with the existing top layer. We refer to such a layer as the 'filling layer', and its nondimensional height is denoted by ζ_f. In contrast, in the step-down scenario, a new layer emerges at the original interface height, and is sandwiched between the lower layer and the existing upper layer. We refer to this new layer as an 'intruding layer', and its nondimensional height is denoted by ζ_i. We allow for entrainment between this layer and the original layer above it through a scaled entrainment flux q_e, as shown in the schematic. It is further assumed for simplicity that q_e is equal to the volume flux of the collapsing relatively dense plume upon arrival at the intruding layer [25]. In either case, the height of the original layer is denoted by ζ_o. One approach to model such flows is to assume temperature is uniform across each layer. We define an appropriately nondimensional scaled temperature θ in (1) below. Using classical plume equations [31] along with conservation of mass and buoyancy (energy) for each layer, Bower et al. [25] developed analytical models to describe both these scenarios.

In our previous study [21] we showed that the analytical model is only valid for a certain regime of parameters for forced ventilation. It was demonstrated that the two nondimensional parameters of inlet volume and momentum flux represent a phase-diagram for which the analytical model based on thorough mixing of each layer is valid. Hence, we restrict our comparison to the intermediate regime that is identified by moderate volume and momentum flux at inlet, which effectively allows for the development of identifiable different layers within the room consistently with the schematic shown in figure 1. Buoyancy flux F is given by $F = g\alpha_V q/(\rho c_p)$, where ρc_p is the heat capacity, and q is the heat load. We use the filling box time as the scaling for time $T_f = \frac{SH}{CFH^{1/3}}$ with C as a universal constant for line plume.

2.1 Governing equations

The flow is governed by Boussinesq equations described below (using Einstein notation)

$$
\begin{aligned}
&\frac{\partial u_j}{\partial x_j} = 0, \\
&\frac{\partial u_i}{\partial \tau} + \frac{\partial u_i u_j}{\partial x_j} + \frac{\partial p_i}{\partial x_i} - Ri\delta_{i2}\theta - \frac{\partial}{\partial x_j}(\frac{1}{Re}\frac{\partial u_i}{\partial x_j}) = 0, \\
&\frac{\partial \theta}{\partial \tau} + \frac{\partial u_j \theta}{\partial x_j} - \frac{\partial}{\partial x_j}(\frac{1}{Pe}\frac{\partial \theta}{\partial x_j}) = 0,\ \theta = \frac{T - T_{ref}}{T_s - T_{ref}},
\end{aligned} \tag{1}
$$

with $\mathbf{u}, p, \theta$ as scaled ensemble-averaged velocity, pressure and temperature, the vertical direction is the second coordinate direction, and δ_{ij} is the Kronecker delta. We use the inlet velocity, V_{in}, height, H, and temperature deficiency of $T_s - T_{ref}$ with T_s as source temperature, as reference values for velocity, length and temperature deficiency, respectively. Nondimensional numbers in Equation set 1 are

$$
Re = \frac{V_{ref} L_{ref}}{\nu_{eff}}, Pe = \frac{V_{ref} L_{ref}}{\kappa_{eff}}, Ri = \frac{g\alpha_V \Delta T_{ref} L_{ref}}{V_{ref}^2}, \tag{2}
$$

where ν_{eff} and κ_{eff} are effective viscosity and diffusivity defined below. Also note that in this study we assume $Pr = 0.71$, which is the Prandtl number of air at room temperature. For nondimensional time $\tau = \frac{t}{T_f}$ we define the characteristic time scale as 'filling time' whose physical meaning and definition is given below.

Boundary conditions are as follows:

$$
\begin{aligned}
&\text{inlet} : u^n = V_{in}, \theta = \theta_{in}, (n_i \partial / \partial x_i) p = 0, \\
&\text{outlet} : (n_i \partial / \partial x_i) u_i = 0, (n_i \partial / \partial x_i)\theta = 0, p = 0, \\
&\text{wall} : \mathbf{u} = 0, (n_i \partial / \partial x_i)\theta = 0, (n_i \partial / \partial x_i) p = 0, \\
&\text{heat load} : \mathbf{u} = 0, \theta = \theta_s, (n_i \partial / \partial x_i) p = 0,
\end{aligned} \tag{3}
$$

where $\mathbf{n}$ is the unit vector normal to the surface and u^n is the normal component of velocity. We consider regimes for which $\frac{T_s - T}{T_s} \ll 1$ so that the Boussinesq approximation is valid and the flow is assumed to be incompressible. We define the scaled inlet temperature $\theta_{in} = \frac{T_{in} - T_{comf}}{T_{comf} - T_s}$. The initial conditions are a steady solution of the system described by Eq. 1 with a quiescent environment for a given heat source prior to step change. We define $\theta_s = \dfrac{T_s - T_{comf}}{T_s(0) - T_{comf}}$, where $T_s(0)$ is the initial temperature of heat load. In this study, we adopt the unsteady RANS (URANS) approach, in which there is a scale separation between the unsteadiness of the mean flow and the turbulence. Using the Boussinesq hypothesis for turbulence and by assuming a constant turbulent Prandtl number, the closure of the system of equations, i.e. the computation of Reynolds stress and turbulent heat flux, is reduced to determining ν_{eff}, for which a standard $k - \epsilon$ closure model is used [32] such that $\nu_{eff} = \nu_t + \nu$. The turbulent heat flux depends on turbulent Prandtl number $Pr_t = 0.9$, which is assumed to be constant for simplicity and is linearly related to ν_t. Finally, the isotropic eddy-diffusivity assumption is implemented to account for the impact of the buoyancy on turbulence. Hence, for a stable and unstable stratification, there is destruction and production of turbulent kinetic energy, respectively.

2.2 Details of Numerical Solver

We use OpenFOAM [22], which is based on a finite-volume method [33] with a collocated grid arrangement and offers object-oriented implementations that suit the employed continuous adjoint formulation (the solver is based on buoyantBoussinesqPimpleFoam). Pressure and velocity are decoupled using the SIMPLE algorithm [34] technique in the state/adjoint equations. For the convection terms, second order Gaussian integration is used with the Sweby limiter [35] to account for propagation of density fronts, and numerical stability. For diffusion, Gaussian integration with central-differencing-interpolation is used. The advective terms in the energy equation are discretized using the second order upwind scheme of the van Leer method [36]. The time integration was performed with the implicit Crank-Nicolson method, which is second-order bounded. The discretized algebraic equations are solved using the Preconditioned biconjugate gradient (PBiCG) method [37]. The mesh sensitivity analysis is discussed in Section 3.

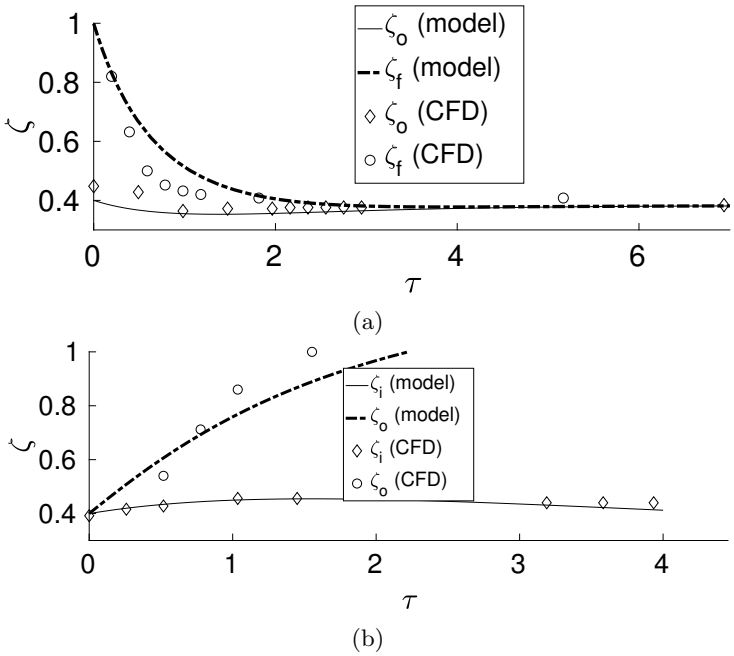

Figure 2: Emptying Filling Box: Interface height based on an analytical model (lines) and numerical simulations (symbols) for: a) step-up of the source (increased F five times); b) step-down of the source (decreased F by a factor of 5). The analytical model has been experimentally validated for this range of parameters [25].

2.3 Numerical Results: Transient Dynamics for a Step Change in Source Strength

In this section, we discuss numerical results from the transient simulations for cases corresponding to both the step-up and step-down scenarios. Note that the inlet flow is kept fixed in both cases. We validate our solver by comparing the results with the experimentally validated mathematical model reported in Bower et al. [25]. The available experimental data for the emptying filling box problem is numerous [23, 24, 38]; however, there is no relevant experimental data for the forced ventilation.

In our previous study [21], we validated our numerical approach by comparing the steady state solutions with corresponding experimental results. In this paper, we are interested in the transient case. Due to similarities of the underlying physical mechanism, we validate our numerical solver by comparing the transient results of our numerical solver with the available experimental data for the emptying filling box case.

2.3.1 Validation of Numerical model for Emptying Filling Box

We focus on the transients in the step-down and step-up scenarios. For the step-up and step-down scenarios, we increased and decreased the buoyancy flux to five times its original value and to 20% of its original value, respectively. The simulation results are compared with the experimental data reported in Bower et al [25]. The results of this comparison are shown in Fig. 2. In both cases, the steady state for a given source strength is set as the initial condition. In the step-up scenario shown in Fig. 2(a), the new descending filling layer merges with the original layer such that the new upper layer consists of a warmer fluid.

For the step-down case, as shown in Fig. 2(b), the upper layer keeps rising, and after a finite time, it leaves the room from the top vents. In the meantime, the upper extent of the new intruding layer ascends up to $\zeta_i = 0.47$ and then descends until it settles down at the (original) steady state interface height. Overall, there is good agreement between the numerical results and the experimentally-validated analytical model for both scenarios. In plotting Fig. 2, we adopt the common practice of defining the interface height as the height at which the the derivative of temperature with respect to height is a local maximum i.e. $\partial T/\partial z = 0$. In some cases where this was not possible due to numerical difficulties, we used alternative reasonable definitions such as the height, at the far left-hand side of the box (away from the plume and the incoming air, say $x = 0.05L$), for which there is (almost) no vertical motion, i.e. $v_y \approx 0$, as is common in the field [24, 25].

2.3.2 Numerical Results for Forced Ventilation

One major difference between the forced ventilation mode and the interior/exterior exchange flow is that the inlet flow conditions in the former situation are not governed by the temperature difference, but rather they are independent variables. Consequently, the steady state interface height in either a step-up or step-down scenario is a function of the source strength. Fig. 3 shows the results of forced ventilation for both step-up and step-down scenarios. In each case, the initial state is the steady state based on a source of $T_s = 305K$. For this simulation, we set the inlet temperature fixed in time as $\theta_{in} = -0.01$. We plot the non-dimensional temperature, where source temperature is set as $T_s(0)$, i.e. the initial source temperature. As shown in Fig. 3(a) for the step-up case, the new filling layer emerges at the top of the domain, and pushes the original layer down. In the step-down scenario shown in Fig. 3(b), an intrusion layer is sandwiched between the rising original layer which is draining through the upper vents, and the lower layer, and, as expected, there is some entrainment from the original layer into this intruding layer. Finally, we notice that in the case of the forced ventilation simulation, i.e. for the results shown in Fig. 3, we keep the inlet temperature fixed in time. In this case, the step-up scenarios result exclusively in filling layers, while the step-down scenarios lead only to intruding layers. On the other hand, as is shown later in the manuscript, in the case of optimal control for which the inlet conditions are time-dependent, these two distinct behaviours do not occur, and both filling and intruding layers may form for either step-up or step-down configurations.

3 Optimal Control Problem : Formulation and Solution Method

In this section, we formally describe the optimal control problem. The region of interest, denoted by Ω, is a rectangular region that spans the length of the room, and reaches up to a specified height ω, which is assumed to be $0.4H$ throughout the paper, without loss of generality, to mimic a typical occupant height in a room. T_{comf} denotes the desired temperature to be maintained in Ω. We set $T_{ref} = T_{comf} = 300K$; however, it should be noted that the analysis is independent of the specific T_{ref} value. The associated scaled temperature for the desired temperature is then $\theta_{comf} = 0$.

We define the cost function as

$$\mathcal{J} = \int_{\Omega}\int_{0}^{\mathcal{T}} \left[\gamma_T \theta(x,y,z,\tau)^2 + \gamma_v \big(\mathbf{v}(x,y,z,\tau) - \mathbf{v}_d\big)^2\right] dV d\tau \tag{4}$$

where $\mathcal{T}$ is the time window during which the optimal control problem is solved, γ_T, γ_v as weighting factors, and $\mathbf{v}_d$ as desired velocity. In this paper, we focused on the thermal comfort problem, for which we assumed $\gamma_T = 1, \gamma_v = 0$. Such a cost function measures the discomfort in the region of interest as the deviation of temperature from T_{comf}. The optimal control problem is then stated as

$$\begin{aligned} \min_{v_{in}(\tau),\theta_{in}(\tau)} \ & \mathcal{J} = \mathcal{J}(\mathcal{W},\mathcal{U}), \\ \text{s.t. } & \mathcal{R}(\mathcal{W},\mathcal{U}) = 0, \end{aligned} \tag{5}$$

where $\mathcal{W} = (\mathbf{u}, p, \theta)$ are the state variables, and $\mathcal{U}$ is the set of control variables, i.e., $\mathcal{U} = (V_{in}, \theta_{in})$. $\mathcal{R}$ denotes the constraints arising from the state governing equations, corresponding to the Boussinesq equations Eq. (1). Additional constraints may also be implemented with no change in the formulation of Eq. (5).

We formulate the optimal control problem using a Lagrangian $\mathcal{L}$ to enforce the Boussinesq equations and constraints, as

$$\min_{v_{in}(\tau),\theta_{in}(\tau)} \mathcal{L} = \mathcal{J} + \langle \mathcal{P}, \mathcal{R} \rangle, \tag{6}$$

where $\mathcal{P} = (\mathbf{v}, p_a, T_a)$ is the vector of adjoint variables, and we use the notation $\langle f, g \rangle = \int_0^{\mathcal{T}} \int_{\mathbb{D}} fg \; dV d\tau$ with $\mathbb{D}$ as the whole domain. It should be noted that we identify time-varying inlet conditions that (locally) minimize $\mathcal{J}$. The adjoint variables are Lagrange multipliers to enforce the state equations Eq. (1). To ensure the (at least local) optimality of the solution, we enforce $\delta\mathcal{L} = \delta_{\mathcal{U}}\mathcal{L} + \delta_{\mathcal{W}}\mathcal{L} = 0$, where δG denotes variation of a dependent variable G. We choose the adjoint variables such that $\delta_{\mathcal{W}}\mathcal{L} = 0$. The sensitivity equations with respect to control variables are then obtained as $\delta\mathcal{L} = \delta_{\mathcal{U}}\mathcal{L}$. This idea is the core of the adjoint method [7, 17, 18] (refer to appendix A for details of our derivation).

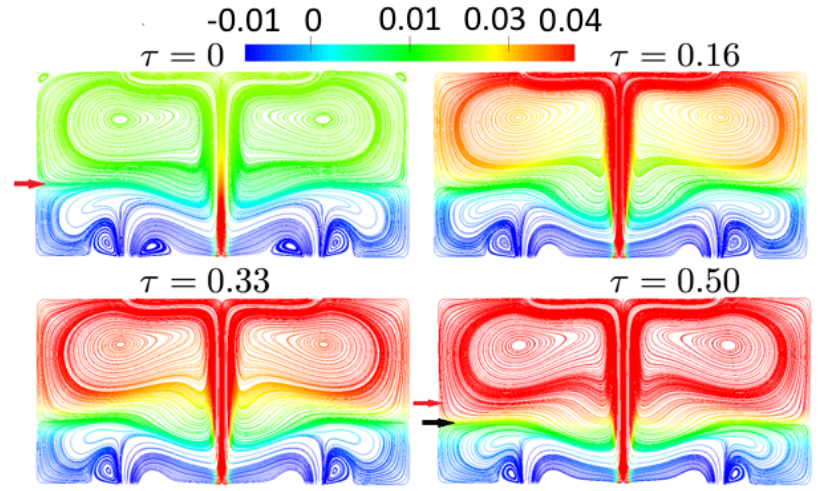

(a)

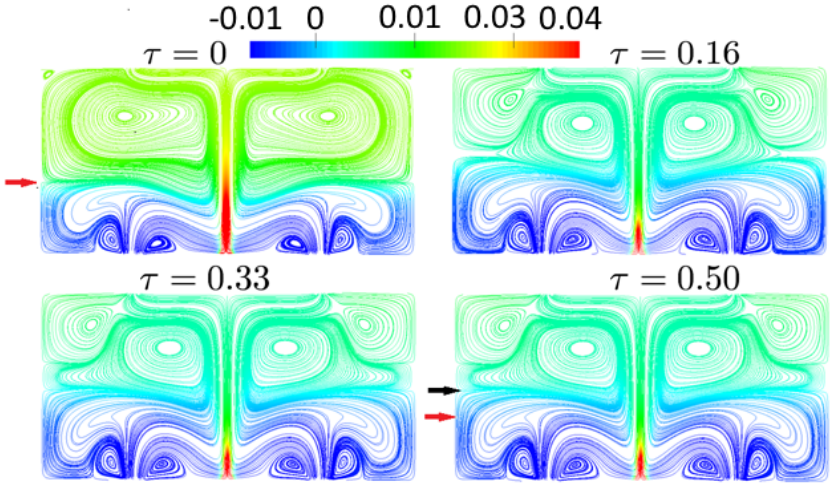

(b)

Figure 3: Forced Ventilation: Streamlines of velocity colored by scaled temperature θ for various times τ. a). Step-up scenario (increased θ_s two times) b). Step-down scenario (decreased θ_s by half). The red arrow in the panels i and iv denotes the original location of the interface, while the black arrow in panel iv denotes the final location of the interface, showing that this interface moves downwards for the step-up case and upwards for step-down case.

By enforcing that first order variations with respect to the state variables vanish at optimal solutions, i.e., $\delta_{\mathcal{W}}\mathcal{L} = 0$, we obtain the adjoint equations

$$\begin{aligned}
&\frac{\partial v_j}{\partial x_j} = 0, \\
&-\frac{\partial v_i}{\partial \tau} + v_j \frac{\partial u_j}{\partial x_i} - u_j \frac{\partial v_i}{\partial x_j} + T_a \frac{\partial \theta}{\partial x_i} - \frac{\partial}{\partial x_j}(\frac{1}{Re}\frac{\partial v_i}{\partial x_j}) + \frac{\partial p_a}{\partial x_i} = 0, \\
&-\frac{\partial T_a}{\partial \tau} - Ri\delta_{i2}v_i - u_j \frac{\partial T_a}{\partial x_j} - \frac{\partial}{\partial x_j}(\frac{1}{Pe}\frac{\partial T_a}{\partial x_j}) + \beta\theta = 0.
\end{aligned} \tag{7}$$

where β is a function that is unity in the region of interest Ω and 0 elsewhere.

The adjoint boundary conditions are

$$\begin{aligned}
&\text{inlet} : \mathbf{v} = 0, T_a = 0, (n_i\partial/\partial x_i)p_a = 0, \\
&\text{outlet} : u^n v^t + \frac{1}{Re}(n_i\partial/\partial x_i)v^t = 0, \\
&T_a u^n + \frac{1}{Pe}(n_i\partial/\partial x_i)T_a = 0, \\
&p_a = u^n v^n + \frac{1}{Re}(n_i\partial/\partial x_i)(v^n), \\
&\text{wall} : \mathbf{v} = 0, (n_i\partial/\partial x_i)T_a = 0, (n_i\partial/\partial x_i)p_a = 0,
\end{aligned} \tag{8}$$

where v^n and v^t are the normal and tangential component of adjoint velocity, respectively.

In deriving Eqs. 7 and 8, we use the 'frozen turbulence' hypothesis [39]; that is we ignore the time variation of turbulent eddies while solving the adjoint equations. In other words, the effective viscosity used in adjoint equations 7 is based on the $k-\epsilon$ fields obtained with the forward system of equations 1. An assessment of the validity of this assumption can be done for a given problem by comparing adjoint sensitivities to those computed using a finite-difference method. We relegate this comparison to appendix B. We refer the reader to [21] for more detailed study on this subject.

The sensitivity of the cost function with respect to inlet velocity and temperature, i.e. the control variables, is obtained as follows.

$$\begin{aligned}
\nabla_{V_{in}}\mathcal{J} &= p_{a,in} - \frac{1}{Re}(n_i\partial/\partial x_i)v_{a,in}, \\
\nabla_{\theta_{in}}\mathcal{J} &= \frac{1}{Pe}(n_i\partial/\partial x_i)T_{a,in},
\end{aligned} \tag{9}$$

where the subscript *'in'* denotes the values at the inlet.

As shown by Nabi et al. [21], the optimization problem favors unboundedly large velocities at inlet, i.e. $v_{in} \to \infty$ with $\theta_{in} = 0$, consistent with the analytical model, in the absence of constraint on the energy budget. To avoid such a nonphysical solution, we enforce an extra constraint on the energy of the incoming flow of the following form:

$$T_{in}V_{in} = d, \tag{10}$$

where d is a given constant value of enthalpy flux at the inlet. The sensitivity Eq. 9 subject to constraint Eq. 10 can be rewritten as

$$\frac{\partial \mathcal{L}}{\partial \theta_{in}} = \nabla_{\theta_{in}}\mathcal{J} - \frac{d}{\theta_{in}^2}\nabla_{V_{in}}\mathcal{J}. \tag{11}$$

In order to update the inlet conditions, we apply a gradient descent method of the form:

$$\theta_{in}^{i+1} = \theta_{in}^{i} - \frac{\partial \mathcal{L}}{\partial \theta_{in}}^{i}, \tag{12}$$

where superscript i denotes the number of iteration.

The optimal control procedure can be summarized as follows:

1. An initial guess for inlet conditions is chosen such that it satisfies Eq. 10. We refer to such an initial guess as θ_{in}^0 whose impact on the DAL results is discussed below.
2. The forward or 'direct' equations are integrated from $\tau = 0$ to $\tau = \mathcal{T}$ by solving Eq. 1. The flow solutions are stored at desired time intervals, named 'checkpoints'. We also evaluate the cost function of Eq. 4.
3. At $\tau = \mathcal{T}$, the initial conditions for the adjoint equations 7 are solved backward in time. Since saving all forward states in memory is not feasible, especially for large $\mathcal{T}$, we use the check-pointing method [17].
4. Once the values for the adjoint variables are obtained at each time, the sensitivities for the constrained optimal control problem are calculated using Eq. 11
5. The next best values of inlet conditions are then found via gradient descent using Eq. 12.
6. The steps 2-5 are repeated until the convergence criteria for the cost functional is satisfied, i.e. $\frac{|\mathcal{J}^{i+1}-\mathcal{J}^i|}{\mathcal{J}^i} \leq \epsilon$. We set the tolerance $\epsilon = 1e-3$.

The adjoint equations are also solved using the numerical method described in Section 2.2 for solving the forward equation. We found that using an upwind and first order method for solving the adjoint equations Eqs. 7 resulted in inaccurate gradients, and hence those methods were not adopted. Refer to appendix B for further validation of adjoint equations.

Finally, for mesh sensitivity analysis, we carried out two separate tests for froward and adjoint equations. In case of the forward simulations, we used the interface height as the monitoring parameter to check the mesh sensitivity between two coarse mesh of 30,800 elements and refined mesh of 147,630 elements. During the time interval of $t \in [0, T_f]$, we noticed that the interface height is less than only 3 percent different between the coarse and refined mesh. For the adjoint equations, on the other hand, sensitivity to the mesh size is much more pronounced, specially in the control region, i.e. the inlet surface in our case. This is also confirmed from 9 where the normal gradient of adjoint velocity and temperature is employed to calculate the gradient of the cost function. Hence, we refined the mesh in particular around the inlet. We have also refined the mesh in the core region of the plume to better capture the ascending dynamics of the plume and the entrainment process. For the mesh sensitivity analysis of the adjoint equations we used $\frac{\partial \mathcal{L}}{\partial \theta_{in}}$ defined in Eq. 11. We realized the sensitivity obtained in the coarse mesh leads to a large error when compared with that of the finite-difference of Eq. 19 introduced in Appendix B. Thus we also considered several intermediate meshes such that the value of $\frac{\partial \mathcal{L}}{\partial \theta_{in}}$ does not alter more than 5 percent between two meshes with the refinement ratio of 1.23. Therefore, the refined mesh of the size 147,630 elements is used in the following DAL simulations, even though much less number of mesh elements are required if only forward simulations were to be considered. Such computationally demanding behavior of the continuous adjoint method is also observed in other references (e.g. see [40]). The minimum of $y+$ is 0.01, the maximum is 3.12, and the average is 0.2837. As we discussed above, the adjoint method demands a very refined mesh and even though the forward problem could be simulated with standard wall functions for which $30 < y+ < 300$ would have been sufficient such that the first cell would reside in the log region, we use the viscous sublayer resolution approach for which the first layer can fall within boundary layer. The Reynolds number for the intermediate regime considered in this study is chosen to make the resolution of viscous sublayer feasible. For large values of Re, the forced convection becomes dominant and the two-layer stratification may not exist. In our simulations, for a typical optimization loop we have $T_{cpu} = 4000s$. This is for the mesh of 147630 elements. We ran the case in parallel mode on 10 Intel Xeon CPUs with 2.40GHz speed. Every DAL iteration loop with checkpointing method requires $3T_{cpu}$ clock time and for a typical optimization about 5 DAL iteration loops are needed to reach to convergence.

4 Results and Discussion

We discuss the solution of the optimal control problem for the step up scenario. The initial state is the optimal steady state solution for $\theta_s = (T_s - T_{comf})/(T_s(0) - T_{comf}) = 1$ with $T_s(0) = 305K$. Note that the optimal solution for the steady-state case is independent of the value chosen as the initial guess of θ_{in}, as shown by [21]. At $\tau = t/T_f = 0$ we increase the source temperature to $\theta_s = 2$. For all optimization problems considered in this paper, the initial guess for the inlet temperature is taken to be a uniform value in time, and denoted by θ_{in}^0. The inlet velocity is then found using the constraint $V_{in}T_{in} = d$. Fig. 4 shows the results associated with various DAL iterations for calculations with $\theta_{in}^0 = -0.01$ (i.e. optimal inlet for $\theta_s = 1$). The source is changed to $\theta_s = 2$ at $\tau = 0$. The time window is taken to be $\mathcal{T} = 0.48$, i.e. about half of the filling time T_f. As shown in Fig. 4(a), at the first iteration of the DAL method, the sensitivity values are large. In subsequent iterations shown in Fig. 4(b-d), the sensitivity decreases, and the time-dependent inlet temperature converges to its optimal structure. Note that at $\tau = \mathcal{T}$ the initial condition

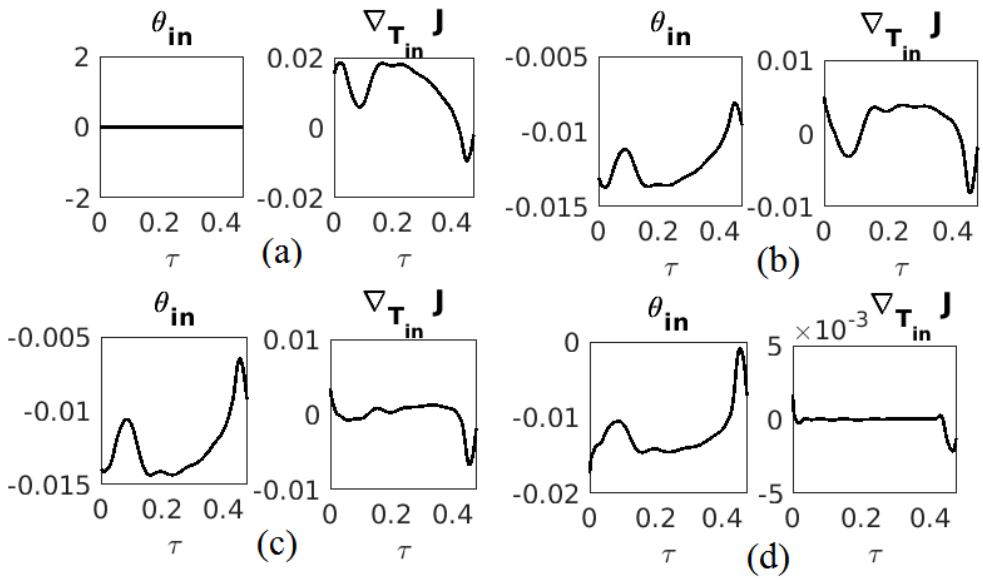

Figure 4: Variation with scaled time τ of the inlet temperature (left panels) and sensitivity of the cost function (right panels) for a DAL method calculation with the initial guess $\theta_{in}^0 = -0.01$ at iteration: a) 1; b) 2; c) 3; and d) 10, when convergence has been achieved. Time window is $\mathcal{T} = 0.48$.

for adjoint equations implies $\nabla_{T_{in}} \mathcal{J} = 0$; therefore, for each iteration we have $\theta_{in}(\mathcal{T}) = \theta_{in}^0$. We found that the cost function of Eq. (4) drops significantly between the first and final iterations of the DAL method, as expected, such that it satisfies the convergence criterion.

In the following, we numerically probe the dependence of the optimal inlet time-dependent functional form θ_{in}^{opt}, and the optimal control cost $\mathcal{J}^{opt}$ on both the initial guess of the inlet temperature, i.e. θ_{in}^0, and the time window $\mathcal{T}$. Robustness of the optimal solution with respect to variations in both the initial guess and the time horizon is clearly important to obtain an effective optimal control scheme.

4.1 Impact of Initial Guess

Fig. 5 shows the optimal inlet temperature θ_{in}^{opt} as a function of time for several different θ_{in}^0 ,i.e. initial guesses values. θ_{in}^0 may be the optimal value corresponding to the source strength prior to the step change. For results of Fig. 5, we use $\theta_{in}^0 = -0.01$. We tested the robustness of the DAL method to the initial guess by using several different values for the initial guess θ_{in}^0. For instance, when the source strength is increased, we expect the new optimal value of inlet temperature to be smaller than the optimal value corresponding to the original heat source strength. However, to put the robustness of the numerical algorithm to the test, we used positive values of θ_{in}^0 as a 'bad' initial guess. The DAL algorithm is still able to find a near-optimal solution. When $\theta_{in}^0 > 0$, the inlet temperature becomes hotter than the lower layer leading to an unstable flow at the inlet, and forms a buoyant plume of its own which may manifest itself as oscillations in the adjoint variables, and eventually in the optimal solution. Such oscillations can be eliminated by penalizing the control action, i.e. $\theta_{in}(\tau)$. In terms of applications, providing oscillatory time variation of temperature or velocity may not be feasible for the device. Alternatively, to smoothen out or to completely remove such oscillations we use a low-pass filter applied to the sensitivity profile at each DAL method iteration to lessen or remove the oscillations. The case of $\theta_{in}^0 = 0.2$ in Fig 5 is shown with the filter applied.

Figs. 6 and 7 show the evolution of the flow for the first and the last DAL method iteration, respectively, when $\theta_{in}^0 = -0.2$. The first iteration shown in Fig. 6 has the bottom layer at a temperature that is lower that the desired value. Also, the formation of an intrusion is evident. For the final iteration of Fig. 7, the lower layer temperature is close to $\theta = 0$, and the height of the interface for most part is close to the top of region of interest, shown with a dashed box. Similarly, for the first DAL method iteration with initial guess of $\theta_{in}^0 = 0.08$ shown Fig. 8, the bottom layer is hotter than the desired value, and the region of interest is mainly filled with buoyant fluid, with no

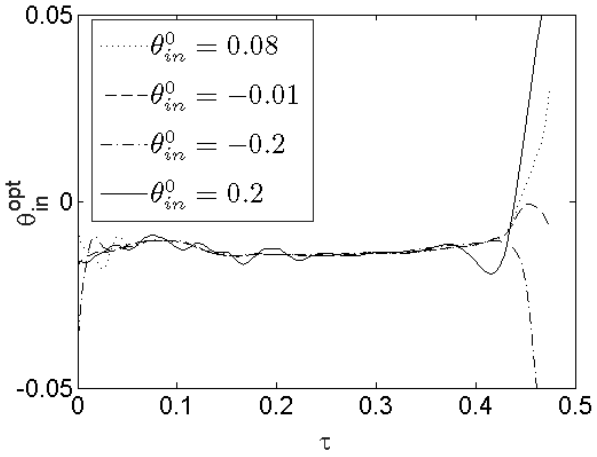

Figure 5: Optimal inlet temperature θ_{in}^{opt} as a function of time for various initial guesses of inlet temperature θ_{in}^0. In all cases shown $\mathcal{T} = 0.48$.

well-defined interface. We find that the converged solution in this case is nevertheless essentially identical to the one for $\theta_{in}^0 = -0.2$ shown in Fig. 7.

Hence, we have demonstrated that the DAL method is successful in finding the optimal control that keeps temperature in the region of interest close to the desired value. The variation of scaled interface height, ζ, with time is shown in Fig. 9 for the first, and final (converged) DAL method iterations. All the optimal controls exhibit similar behavior in terms of interface height. For the initial DAL method iterations, the interface height is significantly below that of the optimal solutions. In fact, for the case where the inlet temperature is too hot, the interface height is not well-defined (also evident in Fig. 8) and this case is not in the 'intermediate regime' identified previously [21]. Up to $\tau = 0.48$, the interface height ζ defined at $x = 0.05L$ becomes almost independent of time in the interval of $0.35 < \tau < 0.48$; see Fig. 9. Hence, such simulation time seems to be long enough to capture the dynamics of the bulk properties of the flow such as the interface height.

4.2 Impact of Time Window

In this section we examine the impact of the time horizon $\mathcal{T}$ on the optimal control $\theta_{in}^{opt}(\tau)$. In Fig. 10, we plot $\theta_{in}^{opt}(\tau)$ for three different time horizons, i.e., $\mathcal{T} = 0.48, 0.96, 1.43$, for the initial guess of $\theta_{in}^0 = -0.01$ and $\theta_s = 2$, i.e. the step-up in the heat source. In each case, there is a sharp gradient near the end of the time horizon to enforce zero sensitivity at final time.

Also shown in Fig. 10 are steady state optimal solutions. The horizontal lines of $\theta_{in} = -0.01, -0.02$ correspond to steady state optimal inlet values corresponding to $\theta_s = 1$ and $\theta_s = 2$, respectively. Note that these solutions have been validated by comparison with analytical model optimization results in [21]. For shorter time-horizons $\mathcal{T}$, the average of θ_{in}^{opt}, i.e. $\bar{\theta}_{in}^{opt} = \frac{\int \theta_{in}^{opt} d\tau}{\mathcal{T}}$, is significantly different from both the steady-state results. In particular, $\bar{\theta}_{in}^{opt} = -0.0122$, -0.0186, and -0.0197 for, respectively, $\mathcal{T} = 0.49$, 0.98, and 1.47. For large enough values of $\mathcal{T}$ the optimal control time-average value converges to the steady state value. Therefore, from a practical point of view, for large times of operation, the steady state results may serve as estimation of the optimal policy whereas for short time horizons of interest, a non-trivially different profile is expected.

4.3 Impact of the Size of Step Change in Source Strength

Fig. 11(a) shows the optimal control solutions corresponding to different sizes of step-up in source strength. As expected, colder inlet temperatures are favored for higher source strengths, consistent with steady state results. It should also be noted that for cases considered in Fig. 11(a), the inlet temperature remains lower than that of the lower layer, and hence oscillations in optimal inlet temperature are minimal. Fig. 11(b) shows the volumetric cost

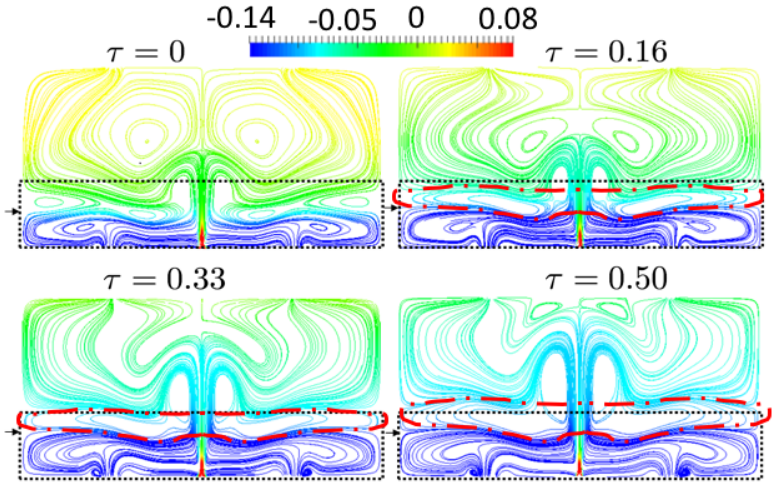

Figure 6: Streamlines of velocity colored by scaled temperature θ for the solution with initial guess of $\theta^0_{in} = -0.2$ for various times τ. This solution corresponds to the first iteration of the DAL method calculations. The dotted box in each figures shows the region of interest, and the arrows mark the determined interface location. The red dashed line at $\tau = 0.16, 0.33$, and 0.50 shows the formation of intruding layer.

function, i.e. $\mathcal{J} \equiv \int_\Omega \theta(x, y, z, \tau)^2 dV$, as a function of time for $\theta_s = 4$ and $\theta_s = 0.5$. We consider two types of control: the initial DAL method iteration corresponding to the constant in time initial guess θ^0_{in}, and the optimal control $\theta^{opt}_{in}(\tau)$ from the final DAL method iteration. For the larger value of the step change in the heat source strength, the difference between the two controls become larger.

4.4 Convergence of the cost functional

For each DAL iteration loop, the cost $\mathcal{J}$ can be computed from Eq. 4 at $\tau = \mathcal{T}$, i.e. at the end of the simulation. To demonstrate the convergence of the optimization method, we plot the cost as a function of the number of iterations in Fig. 12. It can been seen that the cost is reduced significantly, even when the initial guess is significantly different from the comfortable temperature. Also shown in Fig. 12 is the fact that for various initial guess values, the optimal cost functional is almost identical, consistent with the results of plot Fig. 5.

5 Conclusions

We have presented a DAL framework for computing optimal control policies in the built environment for the case of fully turbulent mixed convection flows using RANS models. We have studied the problem of computing controls to maintain desired temperature optimally in a specified region after the heat source strength is suddenly changed, resulting in time-varying inlet velocity and temperature.

The numerical simulation model was validated against an experimental data-set available for the case of natural ventilation. Convergence of the direct-adjoint-looping (DAL) method implementation was studied by varying the initial guess of the inlet temperature, as well as the time-horizon of the optimal control problem. It was found that in the long time-horizon limit, the time-averaged optimal control profile resembles the (steady state) optimal design computed in our previous work [21]. Moreover, our results showed that the clear distinction between step-up leading to 'filling' and step-down leading to 'intruding' layers breaks down in the forced ventilation flows that we consider in this work. In particular, the step-up configuration with time-dependent inlet conditions leads to both filling and intruding layers. The DAL control algorithm behaves in an analogous fashion for step-down scenarios.

5.1 Practical implications and future work

The framework presented here can be used to compute optimal time-varying inlet control strategies if the time-varying heat source properties are known in advance. Approximate optimal control strategies for such a case can also be

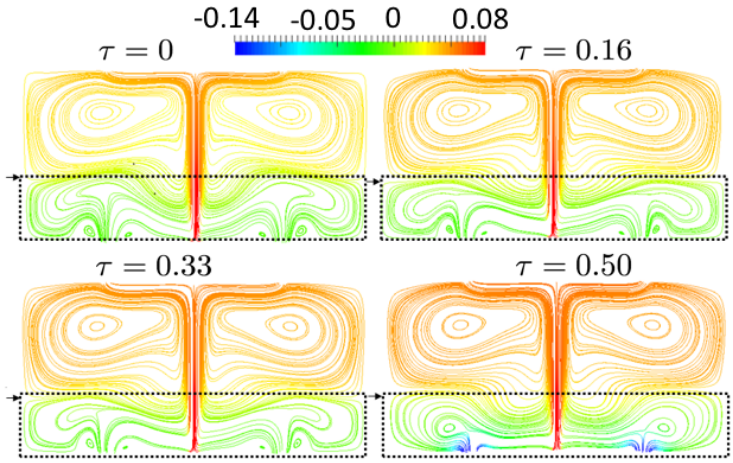

Figure 7: Same as Fig. 6 but the solution corresponds to the last (converged) iteration of the DAL method, i.e. the optimal solution.

computed by linearizing the governing equations, and employing the linear-quadratic (LQR) framework [12]. In such a formulation, the DAL method can be replaced by an operator Riccati equation, and solved in *feedback* form using modern large-scale solvers [41]. It would be interesting to compare and contrast the fully nonlinear DAL method with the linearized approach, to delineate the cases where nonlinear control clearly outperforms linear control, and hence is worth the extra computational cost. Practical implementation of feedback control requires estimation of the full distributed state of the system. Such a task involves building state estimators based on sparse sensing, and is a topic of intense ongoing research [11, 42]. Furthermore, as shown by Kaye and Hunt for emptying filling boxes, the extension to multiple non-interacting plumes is straightforward [24].

As mentioned in the introduction, another intended application of the DAL method framework presented here is to obtain near-optimal open-loop time-periodic (or quasi-periodic) control strategies resulting in flows that are robust to perturbations. In localized heating and cooling applications in large buildings [10], it is crucial to ensure that the associated coherent structures are stable to perturbations, such as those from opening of a window, increase in heating/cooling load, or change in outdoor conditions, etc. This task can benefit from the recent developments in quantifying the stability of time-varying base flows using the nonlinear adjoint framework [43]. Since one often has some knowledge of disturbance locations, inlet strategies can be computed using the DAL method that result in time-varying flows that deviate the least from desired conditions under worst case disturbances. We plan to pursue this topic in the future.

Using a comprehensive thermal comfort model demands consideration of several parameters in addition to air temperature such as airflow velocity, relative humidity, clothing of occupants, and even the mindset of occupants. Quantifying thermal comfort accurately is an ongoing topic of research, see Laftchiev and Nikovski [44]. A detailed consideration of additional parameters in the optimization process, while theoretically possible within the DAL framework, is beyond the scope of the present work.

We used the enthalpy flux of Eq. 10 as representative of energy consumption of the HVAC equipment. A more realistic analysis requires coupling between the building energy systems (BES) and CFD to account for the internal dynamics of air conditioners, e.g., vapor compression systems [45]. A co-simulation approach that considers the dynamical model of the air-conditioner in addition to airflow dynamics governed by Eq. 1 will be considered in future work. This will enable the use of sophisticated performance metrics such as the coefficient of performance (COP) in the optimization process.

Finally, various techniques can be used to speed up the DAL simulation time. For instance, Hazara et al. [46] suggested a 'one-shot' method for steady optimization of Euler equations, and Guenther et al. [47] used simultaneous solution of the forward and adjoint equations in the transient flows with appropriate preconditioning. In future, we aim to adapt and develop a one-shot method for optimization of buoyancy-driven flows. Furthermore, for real-time control one may use reduced-order modeling approaches such as proper orthogonal decomposition (POD) and dynamic mode decomposition (DMD) [42].

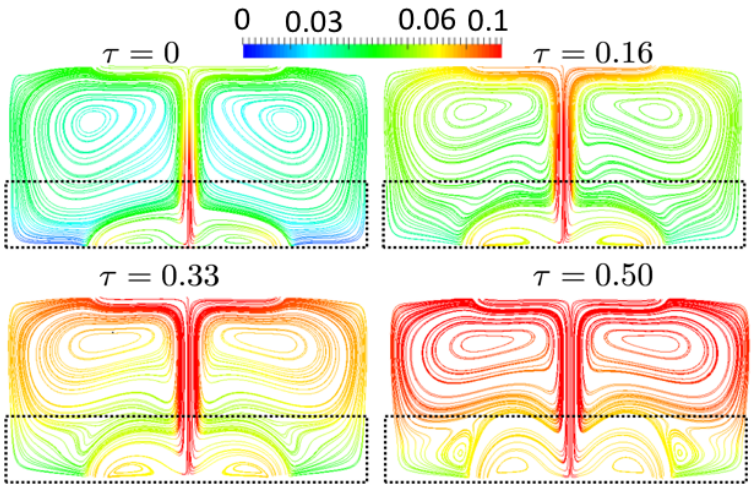

Figure 8: Same as Fig. 6 but for initial guess $\theta^0_{in} = 0.08$. This solution corresponds to the first iteration of the DAL method. Note that there is no identifiable interface with these flow conditions.

Appendix A: Derivation of adjoint equations

The augmented objective functional, i.e. Lagrangian, is

$$\begin{aligned}\mathcal{L} = \mathcal{J} + &< v_i, \frac{\partial u_i}{\partial \tau} + \frac{\partial u_i u_j}{\partial x_j} \\ &+ \frac{\partial p_i}{\partial x_i} - Ri\delta_{i2}\theta - \frac{\partial}{\partial x_j}(\frac{1}{Re}\frac{\partial u_i}{\partial x_j}) > + \\ &< p_a, -\frac{\partial u_j}{\partial x_j} > + \\ &< T_a, \frac{\partial \theta}{\partial \tau} + \frac{\partial u_j \theta}{\partial x_j} - \frac{\partial}{\partial x_j}(\frac{1}{Pe}\frac{\partial \theta}{\partial x_j}) >\end{aligned} \tag{13}$$

with $< . >= \int_0^{\mathcal{T}} \int_{\mathbb{D}} dV d\tau$. The variation of the augmented cost function is

$$\begin{aligned}\delta\mathcal{L} = \delta\mathcal{J} + &< v_i, \frac{\partial \delta u_i}{\partial \tau} + \delta u_j \frac{\partial u_i}{\partial x_j} + u_j \frac{\partial \delta u_i}{\partial x_j} \\ &+ \frac{\partial \delta p_i}{\partial x_i} - Ri\delta_{i2}(\delta\theta) - \frac{\partial}{\partial x_j}(\frac{1}{Re}\frac{\partial \delta u_j}{\partial x_j}) > + \\ &< p_a, -\frac{\partial \delta u_j}{\partial x_j} > + \\ &< T_a, \frac{\partial \delta\theta}{\partial \tau} + \delta u_j \frac{\partial \theta}{\partial x_j} + u_j \frac{\partial \delta\theta}{\partial x_j} - \frac{\partial}{\partial x_j}(\frac{1}{Pe}\frac{\partial \delta\theta}{\partial x_j}) > .\end{aligned} \tag{14}$$

For optimality $\delta\mathcal{L} = 0$ should be satisfied. Each term can be calculated analytically. Specifically, using vector

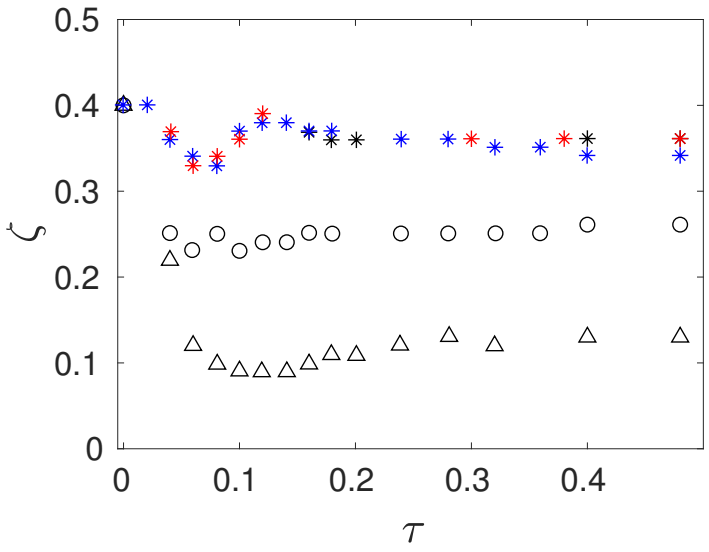

Figure 9: Interface height as a function of time for various cases. The symbols △ mark the case with fixed $\theta^0_{in} = -0.2$, ◯ mark the case with fixed $\theta^0_{in} = 0.08$, while the $*$ mark optimal simulations where the first iteration has $\theta^0_{in} = -0.2$ (black); $\theta^0_{in} = 0.08$ (blue) and $\theta^0_{in} = -0.01$ (red).

calculus and integration by parts, appropriate Euler-Lagrange equations can be derived. For instance,

$$
\begin{aligned}
&< v_i, \frac{\partial \delta u_i}{\partial \tau} >= - < \delta u_i, \frac{\partial v_i}{\partial \tau} > + \int_\Omega v_i(\mathcal{T}) \delta u_i(\mathcal{T}) dV - \\
&\int_\Omega v_i(0) \delta u_i(0) dV \\
&< v_i, \delta u_i \frac{\partial u_j}{\partial x_j} >=< \delta u_i, v_j \frac{\partial u_j}{\partial x_i} > \\
&< v_i, u_j \frac{\partial \delta u_i}{\partial x_j} >= - < \delta u_i, u_j \frac{\partial v_i}{\partial x_j} > + \int v_i \delta u_i u^n dS \\
&< v_i, \frac{\partial}{\partial x_j}(\frac{1}{Re} \frac{\partial \delta u_i}{\partial x_j}) >=< \delta u_i, \frac{\partial}{\partial x_j}(\frac{1}{Re} \frac{\partial v_i}{\partial x_j}) > + \\
&\int \frac{1}{Re}(n_j \frac{\partial v_i}{\partial x_j} \delta u_i - n_j \frac{\partial \delta u_i}{\partial x_j} v_i) dS,
\end{aligned}
\tag{15}
$$

and so on for the other terms. From the space-time integral, the adjoint equations are recovered as

$$
\begin{aligned}
&\frac{\partial v_j}{\partial x_j} = 0, \\
&- \frac{\partial v_i}{\partial \tau} + v_j \frac{\partial u_j}{\partial x_i} - u_j \frac{\partial v_i}{\partial x_j} + T_a \frac{\partial \theta}{\partial x_i} \\
&- \frac{\partial}{\partial x_j}(\frac{1}{Re} \frac{\partial v_i}{\partial x_j}) + \frac{\partial p_a}{\partial x_i} = 0, \\
&- \frac{\partial T_a}{\partial \tau} - Ri \delta_{i2} v_i - u_j \frac{\partial T_a}{\partial x_j} - \frac{\partial}{\partial x_j}(\frac{1}{Pe} \frac{\partial T_a}{\partial x_j}) + \beta \theta = 0.
\end{aligned}
\tag{16}
$$

Setting surface integrals to zero and decomposing these integrals into normal and tangential components, we obtain

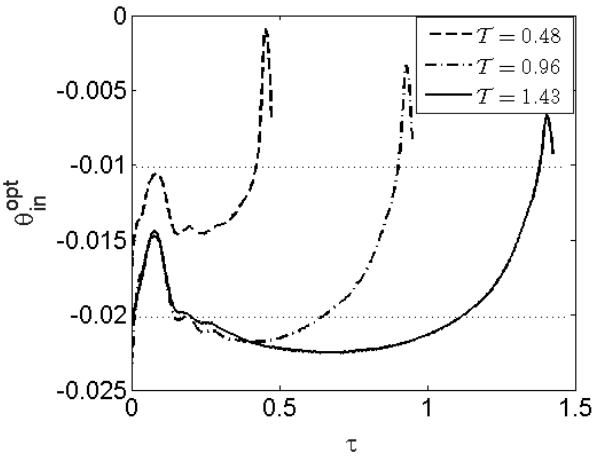

Figure 10: Optimal inlet profile θ_{in}^{opt} as a function of time for various initial values of $\mathcal{T}$. In all cases shown $\theta_{in}^{0} = -0.01$. The horizontal dotted lines are steady-state solutions.

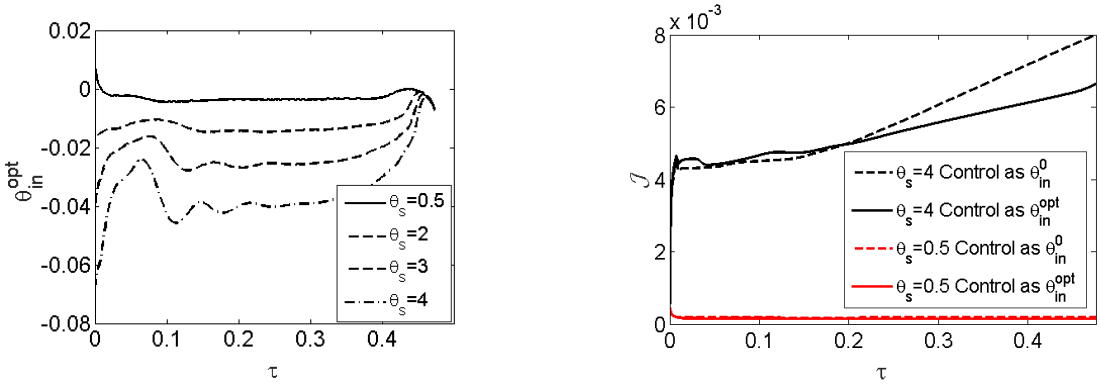

(a) (b)

Figure 11: a) Time dependence of optimal inlet temperature θ_{in}^{opt} for various jumps in the heat load characterized by θ_s. In all cases shown $\theta_{in}^{0} = -0.01$ and $\mathcal{T} = 0.48$. b) V Time dependence of volumetric cost function $\mathcal{J}$ for $\theta_s = 4$ for two types of control; constant inlet conditions of the initial guess θ_{in}^{0} (plotted with dashed lines) and the optimal solution of the DAL method (plotted with solid lines).

$$
\begin{aligned}
(p_a - n_i \frac{1}{Re} \frac{\partial v^n}{\partial x_i} - v^n u^n) &= 0, \\
(n_i \frac{1}{Re} \frac{\partial v^t}{\partial x_i} + v^t u^n) &= 0, \\
(T_a u^n + n_i \frac{1}{Pe} \frac{\partial T_a}{\partial x_i}) &= 0.
\end{aligned}
\tag{17}
$$

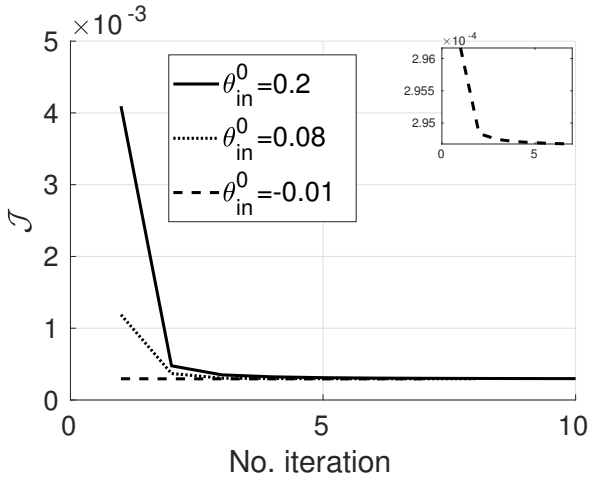

Figure 12: Cost function versus the number of iterations for various initial guesses of inlet temperature θ^0_{in}. The inset figure corresponds to $\theta^0_{in} = -0.01$. In all cases shown $\mathcal{T} = 0.48$.

For each boundary we set the above equations to zero and we obtain the appropriate boundary conditions

$$\begin{aligned}
&\text{inlet} : \mathbf{v} = 0, T_a = 0, (n_i\partial/\partial x_i)p_a = 0 \\
&\text{outlet} : u^n v^t + \frac{1}{Re}(n_i\partial/\partial x_i)v^t = 0, \\
&T_a u^n + \frac{1}{Pe}(n_i\partial/\partial x_i)T_a = 0, \\
&p_a = u^n v^n + \frac{1}{Re}(n_i\partial/\partial x_i)(v^n), \\
&\text{wall} : \mathbf{v} = 0, (n_i\partial/\partial x_i)T_a = 0, (n_i\partial/\partial x_i)p_a = 0.
\end{aligned} \tag{18}$$

Appendix B: validation of sensitivity

We compare the adjoint-based sensitivities, that have been computed using the frozen-turbulence hypothesis, with those computed by a finite-difference (FD) method. Referring to the general first-order forward Euler approximation of a derivative, we obtain

$$\begin{aligned}
\nabla_{V_{in}}\mathcal{J}(\tau)|_{FD} &= \frac{\mathcal{J}(V_{in} + \delta V_{in}, \tau) - \mathcal{J}(V_{in} - \delta V_{in}, \tau)}{2\delta V_{in}}, \\
\nabla_{\theta_{in}}\mathcal{J}(\tau)|_{FD} &= \frac{\mathcal{J}(\theta_{in} + \delta\theta_{in}, \tau) - \mathcal{J}(\theta_{in} - \delta\theta_{in}, \tau)}{2\delta\theta_{in}}.
\end{aligned} \tag{19}$$

In evaluating Eq. 19, the cost function is calculated as follows at time $\tau = \tau_0$: for the time $0 < \tau < \tau_0 - \delta\tau_0$ the forward Eq. 1 are solved with V_{in}, θ_{in} as boundary conditions at the inlet. For the time period $\tau_0 - \delta\tau_0 < \tau < \tau_0 + \delta\tau_0$ the desired perturbation, i.e. δV_{in} or $\delta\theta_{in}$, to inlet boundary conditions are implemented and for the time interval $\tau_o + \delta\tau_0 < \tau < \mathcal{T}$ the boundary conditions are reset as V_{in}, θ_{in}. The value of $\delta\tau_0$ is chosen to be of the order of a time step for the forward solution.

Fig. 13 shows the results of such comparison. Overall, the two methods give similar values for sensitivities. This confirms that our numerical framework is robust, and the assumption of frozen-turbulence in our DAL method does not introduce errors in the computation of optimization problem. Care was taken to choose optimal values for the step size in the finite difference evaluation [21]. Briefly speaking, step size is chosen such that the combination of truncation error and condition error is minimal [48].

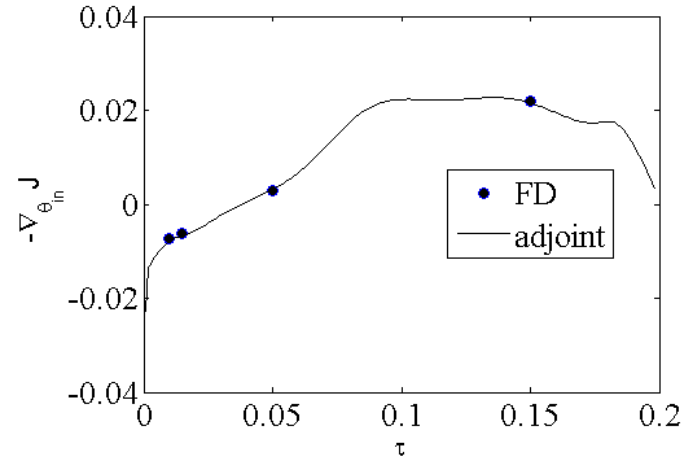

(a)

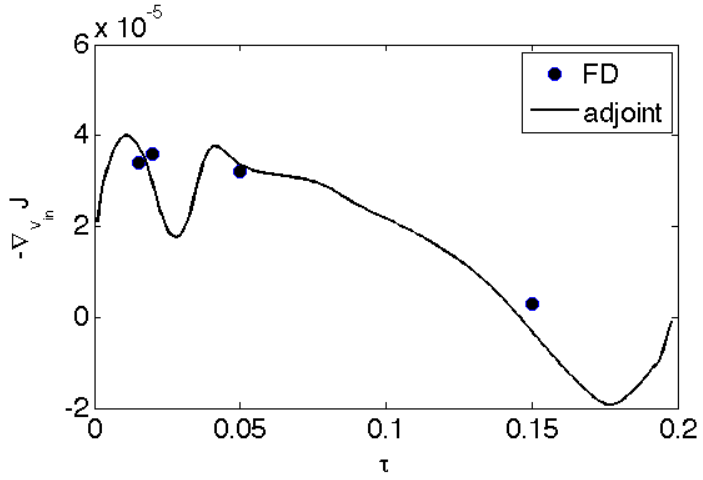

(b)

Figure 13: Comparison of adjoint-based and FD-based sensitivities for validation of the adjoint method. Gradients of the cost function $\mathcal{J}$ with respect to inlet: a) temperature $\nabla_{\theta_{in}}\mathcal{J}$; and b) velocity $\nabla_{V_{in}}\mathcal{J}$ are shown.

References

References

[1] B. A. Cipra, Energy-efficient building design, [Online; accessed 20-February-2017] (2013).
URL `https://sinews.siam.org/Details-Page/energy-efficient-building-design-1/`

[2] P. F. Linden, The fluid mechanics of natural ventilation, Annual review of fluid mechanics 31 (1) (1999) 201–238.

[3] T. R. Bewley, Flow control: new challenges for a new renaissance, Progress in Aerospace sciences 37 (1) (2001) 21–58.

[4] J. E. Peter, R. P. Dwight, Numerical sensitivity analysis for aerodynamic optimization: A survey of approaches, Computers & Fluids 39 (3) (2010) 373–391.

[5] W. K. Anderson, V. Venkatakrishnan, Aerodynamic design optimization on unstructured grids with a continuous adjoint formulation, Computers & Fluids 28 (4) (1999) 443–480.

[6] R. Lanzafame, M. Messina, Fluid dynamics wind turbine design: Critical analysis, optimization and application of bem theory, Renewable energy 32 (14) (2007) 2291–2305.

[7] C. Othmer, A continuous adjoint formulation for the computation of topological and surface sensitivities of ducted flows, International Journal for Numerical Methods in Fluids 58 (8) (2008) 861–877.

[8] M. D. Gunzburger, Sensitivities, adjoints and flow optimization, International Journal for Numerical Methods in Fluids 31 (1) (1999) 53–78.

[9] E. Turgeon, D. Pelletier, J. Borggaard, A continuous sensitivity equation approach to optimal design in mixed convection, Numerical Heat Transfer: Part A: Applications 38 (8) (2000) 869–885.

[10] L. J. Lo, A. Novoselac, Localized air-conditioning with occupancy control in an open office, Energy and Buildings 42 (7) (2010) 1120–1128.

[11] J. A. Burns, J. Borggaard, E. Cliff, L. Zietsman, An optimal control approach to sensor/actuator placement for optimal control of high performance buildings, International High Performance Buildings Conference.

[12] J. A. Burns, W. Hu, Approximation methods for boundary control of the boussinesq equations, in: Decision and Control (CDC), 2013 IEEE 52nd Annual Conference on, IEEE, 2013, pp. 454–459.

[13] J. Borggaard, J. A. Burns, A. Surana, L. Zietsman, Control, estimation and optimization of energy efficient buildings, in: American Control Conference, 2009. ACC'09., IEEE, 2009, pp. 837–841.

[14] W. Liu, Q. Chen, Optimal air distribution design in enclosed spaces using an adjoint method, Inverse Problems in Science and Engineering 23 (5) (2015) 760–779.

[15] S. Zhang, Y. Cheng, C. Huan, Z. Lin, Heat removal efficiency based multi-node model for both stratum ventilation and displacement ventilation, Building and Environment 143 (2018) 24–35.

[16] P. Luchini, A. Bottaro, Adjoint equations in stability analysis, Annual Review of fluid mechanics 46.

[17] R. Kerswell, C. Pringle, A. Willis, An optimization approach for analysing nonlinear stability with transition to turbulence in fluids as an exemplar, Reports on Progress in Physics 77 (8) (2014) 085901.

[18] D. Foures, C. Caulfield, P. J. Schmid, Optimal mixing in two-dimensional plane poiseuille flow at finite péclet number, Journal of Fluid Mechanics 748 (2014) 241–277.

[19] F. Fang, C. Pain, I. Navon, D. Cacuci, X. Chen, The independent set perturbation method for efficient computation of sensitivities with applications to data assimilation and a finite element shallow water model, Computers & Fluids 76 (2013) 33–49.

[20] C. Saglietti, P. Schlatter, A. Monokrousos, D. S. Henningson, Adjoint optimization of natural convection problems: differentially heated cavity, Theoretical and Computational Fluid Dynamics 31 (5-6) (2017) 537–553.

[21] S. Nabi, P. Grover, C.-c. P. Caulfield, Adjoint-based optimization of displacement ventilation flow, Building and Environment 124 (2017) 342–356.

[22] OpenFOAM - the open source computational fluid dynamics (cfd) toolbox, `http://openfoam.com`.

[23] P. Linden, G. Lane-Serff, D. Smeed, Emptying filling boxes: the fluid mechanics of natural ventilation, Journal of Fluid Mechanics 212 (1990) 309–335.

[24] N. Kaye, G. Hunt, Time-dependent flows in an emptying filling box, Journal of Fluid Mechanics 520 (2004) 135–156.

[25] D. Bower, C. Caulfield, S. Fitzgerald, A. Woods, Transient ventilation dynamics following a change in strength of a point source of heat, Journal of Fluid Mechanics 614 (2008) 15.

[26] S. Nabi, M. Flynn, Influence of geometric parameters on the eventual buoyancy stratification that develops due to architectural exchange flow, Building and Environment 71 (2014) 33–46.

[27] S. Nabi, M. Flynn, Buoyancy-driven exchange flow between two adjacent building zones connected with top and bottom vents, Building and Environment 92 (2015) 278–291.

[28] J. Craske, M. van Reeuwijk, Generalised unsteady plume theory, Journal of Fluid Mechanics 792 (2016) 1013–1052.

[29] S. Meerkov, Principle of vibrational control: Theory and applications, IEEE Transactions on Automatic Control 25 (4) (1980) 755–762.

[30] S. S. Collis, R. D. Joslin, A. Seifert, V. Theofilis, Issues in active flow control: theory, control, simulation, and experiment, Progress in aerospace sciences 40 (4-5) (2004) 237–289.

[31] B. Morton, G. I. Taylor, J. S. Turner, Turbulent gravitational convection from maintained and instantaneous sources, Proceedings of the Royal Society of London. Series A. Mathematical and Physical Sciences 234 (1196) (1956) 1–23.

[32] B. Mohammadi, O. Pironneau, Analysis of the k-epsilon turbulence model.

[33] H. G. Weller, G. Tabor, H. Jasak, C. Fureby, A tensorial approach to computational continuum mechanics using object-oriented techniques, Computers in physics 12 (6) (1998) 620–631.

[34] S. V. Patankar, D. B. Spalding, A calculation procedure for heat, mass and momentum transfer in three-dimensional parabolic flows, International journal of heat and mass transfer 15 (10) (1972) 1787–1806.

[35] P. K. Sweby, High resolution schemes using flux limiters for hyperbolic conservation laws, SIAM journal on numerical analysis 21 (5) (1984) 995–1011.

[36] B. Van Leer, Towards the ultimate conservative difference scheme. ii. monotonicity and conservation combined in a second-order scheme, Journal of computational physics 14 (4) (1974) 361–370.

[37] J. H. Ferziger, M. Peric, A. Leonard, Computational methods for fluid dynamics (1997).

[38] S. Nabi, M. Flynn, The hydraulics of exchange flow between adjacent confined building zones, Building and Environment 59 (2013) 76–90.

[39] E. Papoutsis-Kiachagias, K. Giannakoglou, Continuous adjoint methods for turbulent flows, applied to shape and topology optimization: industrial applications, Archives of Computational Methods in Engineering 23 (2) (2016) 255–299.

[40] A. Önder, J. Meyers, Optimal control of a transitional jet using a continuous adjoint method, Computers & Fluids 126 (2016) 12–24.

[41] P. Benner, J.-R. Li, T. Penzl, Numerical solution of large-scale lyapunov equations, riccati equations, and linear-quadratic optimal control problems, Numerical Linear Algebra with Applications 15 (9) (2008) 755–777.

[42] B. Kramer, P. Grover, P. Boufounos, S. Nabi, M. Benosman, Sparse sensing and DMD-based identification of flow regimes and bifurcations in complex flows, SIAM Journal on Applied Dynamical Systems 16 (2) (2017) 1164–1196.

[43] R. Kerswell, Nonlinear nonmodal stability theory, Annual Review of Fluid Mechanics 50 (1).

[44] E. Laftchiev, D. Nikovski, An iot system to estimate personal thermal comfort, in: 2016 IEEE 3rd World Forum on Internet of Things (WF-IoT), IEEE, 2016, pp. 672–677.

[45] H. Qiao, X. Han, S. Nabi, C. R. Laughman, Coupled simulation of a room air-conditioner with cfd models for indoor environment, in: Proceedings of the 13th International Modelica Conference, Regensburg, Germany, March 4–6, 2019, no. 157, Linköping University Electronic Press, 2019.

[46] S. Hazra, V. Schulz, J. Brezillon, N. Gauger, Aerodynamic shape optimization using simultaneous pseudo-timestepping, Journal of Computational Physics 204 (1) (2005) 46–64.

[47] S. Guenther, N. R. Gauger, Q. Wang, Simultaneous single-step one-shot optimization with unsteady pdes, Journal of Computational and Applied Mathematics 294 (2016) 12–22.

[48] J. Iott, R. T. Haftka, H. M. Adelman, Selecting step sizes in sensitivity analysis by finite differences, NASA Technical Memorandum, 1985.